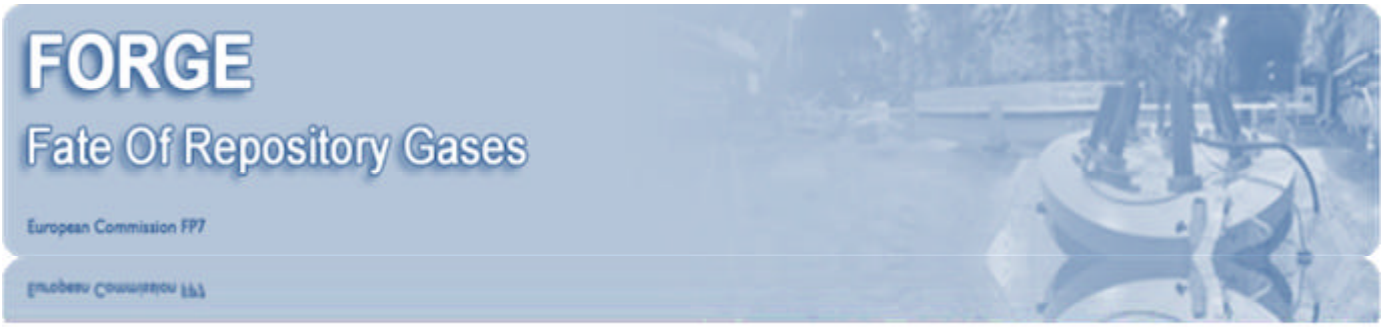


# Results of the tests on bentonite (Part 1)

FORGE Report D3.15 – VER.1

| | Name | Organisation | Signature | Date |
|---|---|---|---|---|
| Compiled | M.V. Villar | CIEMAT | | 7th October 2011 |
| Verified | | | | |
| Approved | | | | |

*Keywords*

.

*Bibliographical reference*

M.V. Villar, P.L. Martín, F.J. Romero, J.M. Barcala. 2012. Results of the tests on bentonite (Part 1). FORGE Report D3.15. 30pp.

Euratom 7th Framework Programme Project: FORGE

## Fate of repository gases (FORGE)

The multiple barrier concept is the cornerstone of all proposed schemes for underground disposal of radioactive wastes. The concept invokes a series of barriers, both engineered and natural, between the waste and the surface. Achieving this concept is the primary objective of all disposal programmes, from site appraisal and characterisation to repository design and construction. However, the performance of the repository as a whole (waste, buffer, engineering disturbed zone, host rock), and in particular its gas transport properties, are still poorly understood. Issues still to be adequately examined that relate to understanding basic processes include: dilational versus visco-capillary flow mechanisms; long-term integrity of seals, in particular gas flow along contacts; role of the EDZ as a conduit for preferential flow; laboratory to field up-scaling. Understanding gas generation and migration is thus vital in the quantitative assessment of repositories and is the focus of the research in this integrated, multi-disciplinary project. The FORGE project is a pan-European project with links to international radioactive waste management organisations, regulators and academia, specifically designed to tackle the key research issues associated with the generation and movement of repository gasses. Of particular importance are the long-term performance of bentonite buffers, plastic clays, indurated mudrocks and crystalline formations. Further experimental data are required to reduce uncertainty relating to the quantitative treatment of gas in performance assessment. FORGE will address these issues through a series of laboratory and field-scale experiments, including the development of new methods for up-scaling allowing the optimisation of concepts through detailed scenario analysis. The FORGE partners are committed to training and CPD through a broad portfolio of training opportunities and initiatives which form a significant part of the project.

Further details on the FORGE project and its outcomes can be accessed at www.FORGEproject.org.

*Contact details:*

**María Victoria Villar**
**CIEMAT**
Tel: +34 913466139 Fax +34 913466542
email: mv.villar@ciemat.es
web address: http://www.ciemat.es/portal.do
Address: Avd. Complutense 22, 28040 Madrid

**Pedro Luis Martín**
**CIEMAT**
Tel: +34 913466142 Fax +34 913466542
email: pedro.lmartin@ciemat.es
web address: http://www.ciemat.es/portal.do
Address: Avd. Complutense 22, 28040 Madrid

**Francisco Javier Romero**
**CIEMAT**
Tel: +34 913462584 Fax +34 913466542
email: francisco.romero@ciemat.es
web address: http://www.ciemat.es/portal.do
Address: Avd. Complutense 22, 28040 Madrid

**José Miguel Barcala**
**CIEMAT**
Tel: +34 913467859 Fax +34 913466542
email: miguel.barcala@ciemat.es
web address: http://www.ciemat.es/portal.do
Address: Avd. Complutense 22, 28040 Madrid

# Foreword

This report includes the work performed by CIEMAT in WP3.2 “Gas permeability and breakthrough pressure as a function of dry density, water content and pressure in buffer materials” and WP3.3 “Gas transport through joints between buffer blocks and between host rock/buffer”. All the laboratory work included was performed at CIEMAT facilities.

# Acknowledgements

The laboratory work was performed by Ramón Campos and Juan Aroz, from CIEMAT.

# Contents



**FIGURES**

**TABLES**



# Summary

The gas permeability of the Spanish FEBEX bentonite compacted at dry densities of between 1.4 and 1.8 g/cm$^3$ with high water contents was measured for different confining, injection and backpressures. The results were compared with results obtained in previous investigations for lower degrees of saturation. It was checked that gas permeability was greatly affected by dry density, decreasing about three orders of magnitude when it increased from 1.5 to 1.8 g/cm$^3$ for similar water content. The increase of water content caused also a decrease in gas permeability. It was found that both gas permeability and the relative gas permeability were mainly related to the accessible porosity. These relationships could be fitted to potential expressions with exponents between 3 and 4, as well as the relationship between intrinsic permeability and void ratio.

For gas pressures below 12 bar no effect of the injection or confining pressures on the value of permeability was detected, although when confining pressure increased from 10 to 30 bar, the permeability decreased almost two orders of magnitude. For a given confining pressure the permeability value decreased as the effective pressure increased, especially if the increase in effective pressure was due to a decrease in gas backpressure.

It was checked that the Klinkenberg effect was not significant for this material in the range of pressures applied in the tests.

Preliminary results indicated that the breakthrough pressure for the saturated bentonite with a dry density of 1.73 g/cm$^3$ was higher than 10 MPa, whereas for the saturated bentonite with a dry density slightly higher than 1.4 g/cm$^3$ was about 5 MPa. A saturated granite/bentonite interface (bentonite dry density 1.56 g/cm$^3$) allowed the passage of gas under a pressure of 0.7 MPa. After resaturation of this interface, the same breakthrough pressure was found.

# 1 Introduction

This report includes the work performed by CIEMAT in WP3.2 "Gas permeability and breakthrough pressure as a function of dry density, water content and pressure in buffer materials" and WP3.3 "Gas transport through joints between buffer blocks and between host rock/buffer". The buffer material used in the tests is the Spanish FEBEX bentonite, and granite has been used as host rock.

# 2 Material

The FEBEX bentonite was extracted from the Cortijo de Archidona deposit (Almería, Spain) and the processing at the factory consisted in disaggregation and gently grinding, drying at 60°C and sieving by 5 mm. The physico-chemical properties of the FEBEX bentonite, as well as its most relevant thermo-hydro-mechanical and geochemical characteristics obtained during the projects FEBEX I and II are summarised in the final reports of the project (ENRESA 2000, 2006). A summary of the results obtained is given below.

The montmorillonite content of the FEBEX bentonite is above 90 wt.% (92±3 %). The smectitic phases are actually made up of a smectite-illite mixed layer, with 10-15 wt.% of illite layers. Besides, the bentonite contains variable quantities of quartz (2±1 wt.%), plagioclase (3±1 wt.%), K-felspar (traces), calcite (1±0.5 wt.%), and cristobalite-trydimite (2±1 wt.%).

The cation exchange capacity is 102±4 meq/100g, the main exchangeable cations being calcium 35±2 meq/100g, magnesium 31±3 meq/100g and sodium 27±1 meq/100g. The predominant soluble ions are chloride, sulphate, bicarbonate and sodium.

The liquid limit of the bentonite is 102±4 %, the plastic limit 53±3 %, the density of the solid particles 2.70±0.04 g/cm$^3$, and 67±3 % of particles are smaller than 2 μm. The hygroscopic water content in equilibrium with the laboratory atmosphere (relative humidity 50±10 %, temperature 21±3 °C, total suction about 100 MPa) is 13.7±1.3 %. The external specific surface area is 32±3 m$^2$/g and the total specific surface area is about 725 m$^2$/g.

The saturated hydraulic conductivity of compacted bentonite samples is exponentially related to their dry density. For a dry density of 1.6 g/cm$^3$ the saturated permeability of the bentonite is about $5 \cdot 10^{-14}$ m/s at room temperature, with deionised water used as percolating fluid.

The swelling pressure of compacted samples is also exponentially related to the bentonite dry density, and when the bentonite at dry density of 1.6 g/cm$^3$ is saturated with deionised water at room temperature, the swelling pressure has a value of about 6 MPa.

The retention curve of the bentonite was determined in samples compacted to different dry densities at different temperatures (Lloret et al., 2004; Villar & Gómez-Espina 2009). The volume of the samples remained constant during the determinations, since they were confined in constant volume cells.

Some isothermal infiltration tests and heat flow tests at constant overall water content were performed during the FEBEX I project (ENRESA 2000, 2006) and they were backanalysed using CODEBRIGHT. The experimental data were fitted using a cubic law for the relative permeability and a value of 0.8 for the tortuosity factor.

# 3 Methodology

Different kinds of tests were performed: gas permeability tests, breakthrough tests and tests in interfaces. The buffer material used in all of them is the FEBEX bentonite compacted at different dry densities.

## 3.1 GAS PERMEABILITY

Gas permeability was measured in specimens of compacted FEBEX bentonite. Prior to compaction (several days earlier), the granulated bentonite was mixed with different quantities of deionised water, in order to obtain water contents of between 18 and 22%. Cylindrical samples of 3.8 cm diameter and 7.8 cm height were obtained by uniaxial compaction of the wet bentonite. Compaction pressures of between 30 and 152 MPa were applied to manufacture specimens of dry densities of between 1.4 and 1.8 g/cm$^3$.

The cylindrical samples were placed in a triaxial cell confined between two porous stones and wrapped in two latex membranes, between which vacuum grease was applied in order to prevent the loss of gas. The cell walls were made of methacrylate and were capable of withstanding pressures up to 3 MPa (Figure 1). The cells had four inlets drilled in the base, one for the sample top drainage/back pressure, two for the sample bottom drainage/pore pressure, and one for the confining pressure. In one of the tests (test FBX16), a stainless steel triaxial cell able to withstand pressures of up to 20 MPa was used.

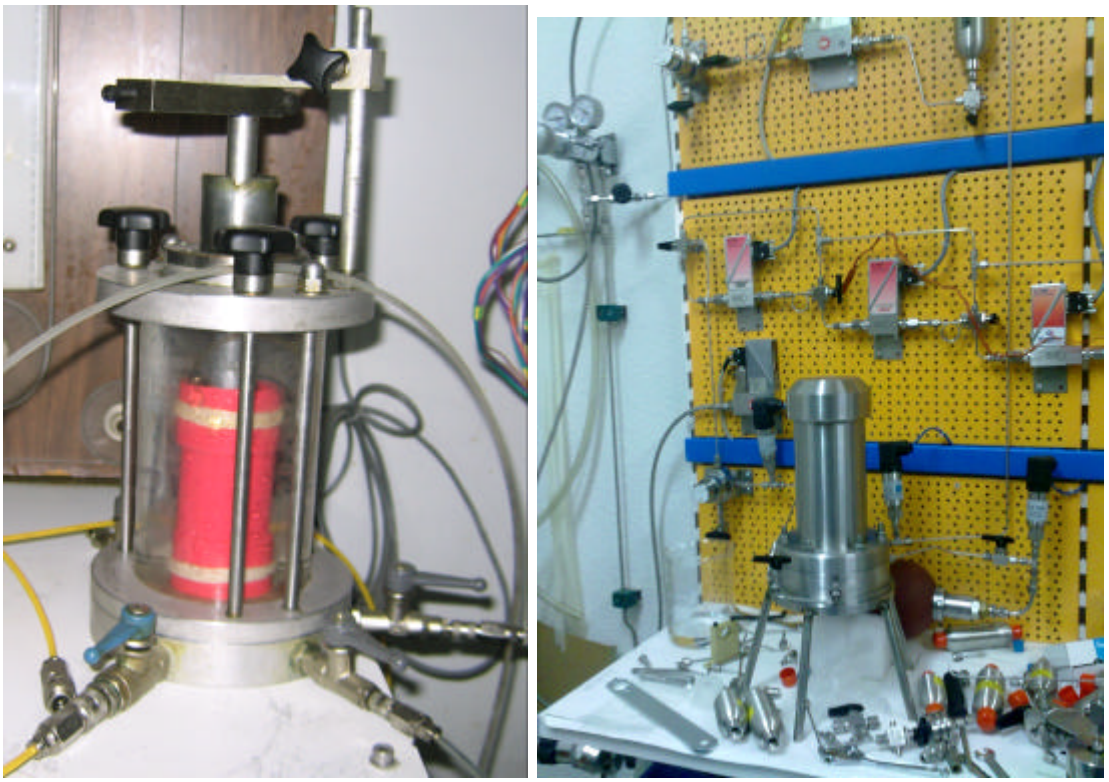

**Figure 1: Bentonite sample inside a methacrylate triaxial cell (left) and high-pressure cell (right)**

The setup to perform gas permeability measurements was designed to work as a constant head permeameter under different gas pressures, with the possibility to change the head value and measure the gas inflow and outflow (Figure 2). The cell was filled with water and pressurised with nitrogen, which was separated from the water in the cell through an elastic membrane contained in an OLAER's pressure accumulator capable of withstanding pressures of up to 330

bar. The injection and downstream pressures could be independently varied and kept constant during the period of time necessary to get steady flow by HI-TEC gas forward pressure controllers. Associated to the pressure controllers, DRUCK pressure transmitters (PTX1400 series, 100 bar a, 0.15% typical accuracy, overpressure 2 x FS), were placed for redundancy at the inlet and outlet of the cell. Different range HITECH gas mass flowmeters measured the inward and outward flows (0.2-10, 2-100 and 20-1000 STP $cm^3$/min). Gas mass flowmeters were used to prevent the potential impact of deviation from the ideal behaviour of gas on the measurement of the molecular flow rate and, hence, on the calculated permeability coefficients. Nitrogen gas was used as fluid. The technical details of the equipment were given in Villar *et al*. (2010).

The system applied the pressures to the sample and registered flow and pressures from the measurement devices. In and outflow gas rates, up and downstream pressure, temperatures and the confining pressure were monitored.

After all the gas permeability measurements were performed, the setup was modified and divided into two separate measurement lines that were used for the breakthrough tests and for the tests in interfaces. In the new version of the setup, the backpressure was kept atmospheric and only the gas outflow was measured (by means of different range HITECH gass flowmeters).

To compute the permeability (intrinsic permeability measured with gas flow, $k_{ig}$, relative permeability to gas, $k_{rg}$) the inflow or outflow measurements can be used, applying the following equation for incompressible media with compressible pore fluids (Scheidegger 1974):

$$k_{ig} \cdot k_{rg} = \frac{Q_m \times m_g \times L \times 2P_m}{A \times (P_{up}^2 - P_{dw}^2)} \quad [1]$$

where $Q_m$ is the measured flow (volume of fluid as a function of time), $A$ is the sample surface area, $\mu_g$ is the fluid dynamic viscosity, $L$ is the sample length and $P_{up}$ and $P_{dw}$ are the upstream and downstream pressures applied at the top (inlet) and the bottom (outlet), respectively, of the sample, and $P_m$ is the pressure of the measured flow (in our case, due to the STP conditions of the gas mass flowmeters, the atmospheric pressure). In turn gas permeability, $k_g$, can be computed taking into account the gas density and viscosity change with upstream or downstream pressures ($P$):

$$k_g = \frac{r_g \times g \times P}{m_g} \times k_{ig} \times k_{rg} \quad [2]$$

It is considered that the viscosity of nitrogen did not change during the tests because they were isothermal, whereas density changed with pressure. The change in density was considered as that of an ideal gas, and thus computed as the product of the density of nitrogen at atmospheric pressure times the pressure, either the injection or the backpressure, depending on what flow was used for the computation. This solution assumed that steady state flow was established, what meant that the quantity of gas exiting the sample in the low pressure side was equal to that entering the sample in the high pressure side. This aspect was verified in the tests performed to measure the bentonite gas permeability. In any case, the underestimation of the calculated permeability coefficients should be less than 1.3%.

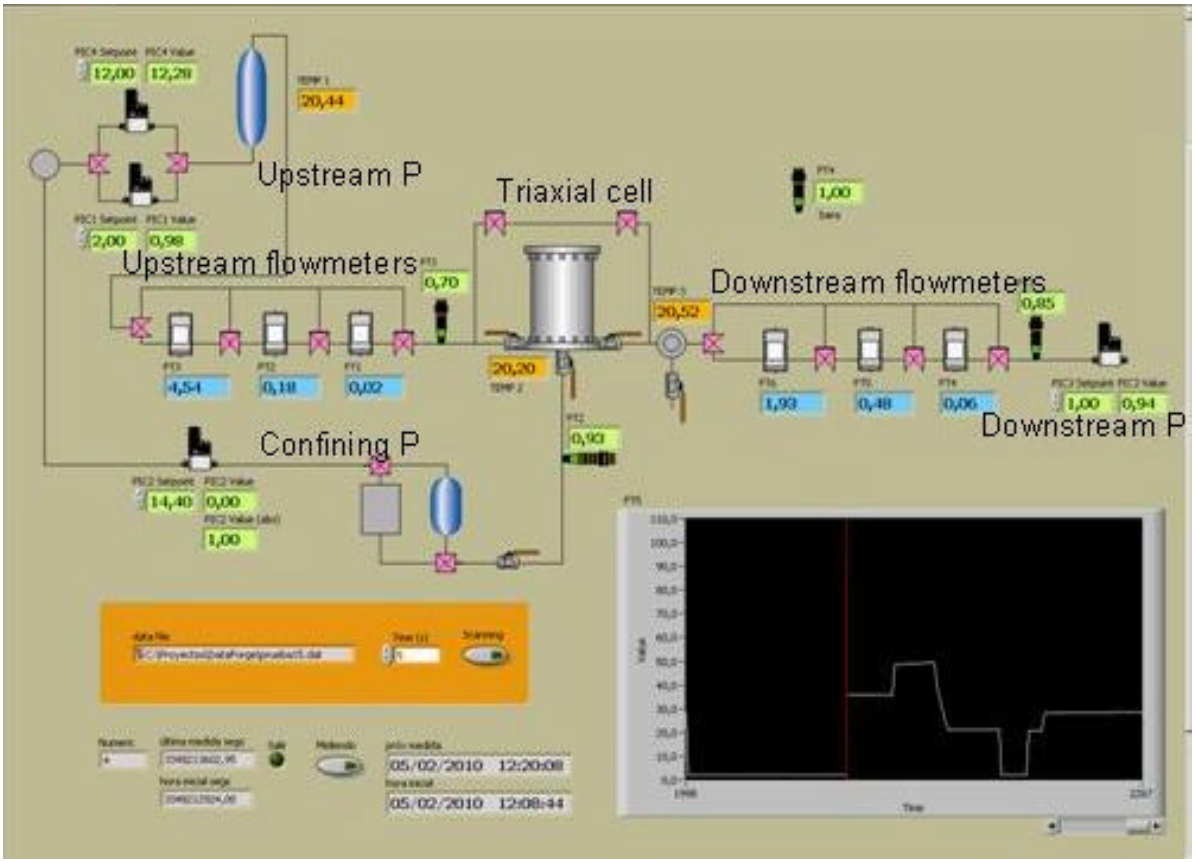


**Figure 2: Schematic diagram of the setup for the gas permeability tests before modification**

To analyse the effect of injection, back and confining pressures on permeability, the tests consisted of several steps, that followed the paths shown in Figure 3:

- Stage 1: under constant confining (6 bar) and backpressure (atm), the injection pressure was increased in steps.
- Stage 2: under constant injection (4 bar) and backpressure (atm), the confining pressure was increased from 6 to 10 bar.
- Stage 3: under constant confining (10 bar) and backpressure (atm), the injection pressure was increased in steps.
- Stage 4: under constant confining (10 bar) and injection pressures (8 bar), backpressure was increased in steps.
- Stage 5: finally, the injection and backpressures decreased simultaneously under constant confining pressure (10 bar).

In test FBX14, after these five stages, the confining pressure was increased to 12 bar and the effect of changing both the injection and the backpressure under this confining pressure was checked. Test FBX16 was performed in a stainless steel cell (Figure 1, right) in order to be able to apply higher injection pressures, since the sample had a very high initial water degree of saturation. The backpressure was kept atmospheric all through the test, while the confining and injection pressures followed the path shown in Figure 4.

At the end of the tests, the bentonite specimens were measured and weighed and the water content was determined by oven-drying at three different levels along the cylinders.

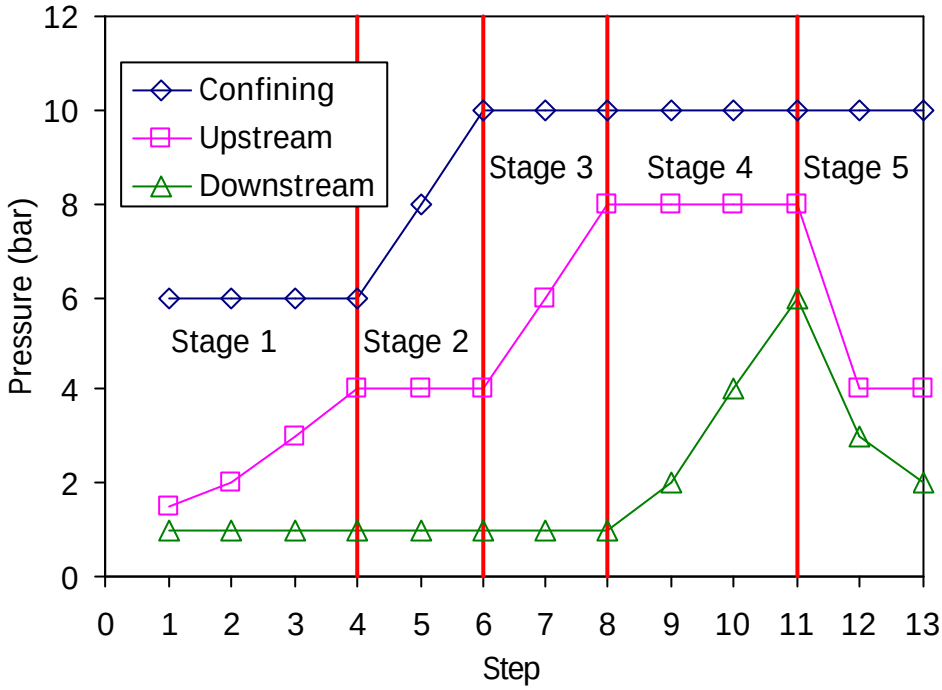


**Figure 3: Pressure paths followed during the gas permeability tests PGFBX3 to PGFBX14**

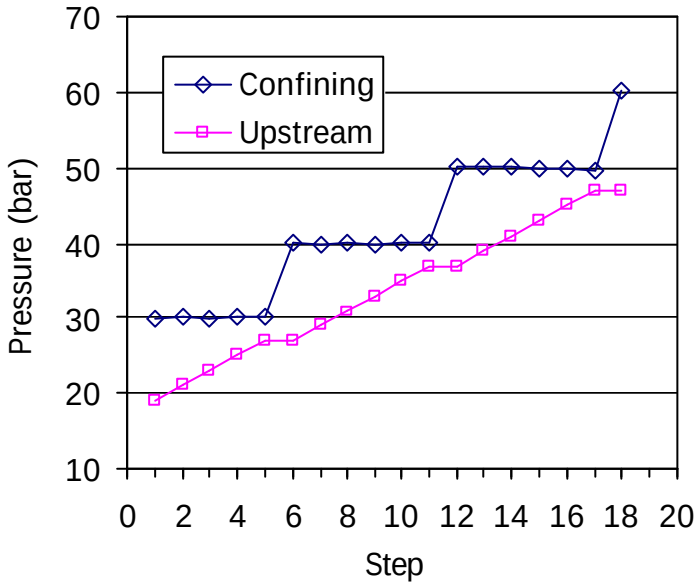


**Figure 4: Pressure path followed during the gas permeability test FBX16. Backpressure was kept atmospheric**

## 3.2 BREAKTHROUGH TESTS

To perform these tests cylindrical bentonite samples were obtained by uniaxial compaction and saturated with deionised water. Two different cells and procedures were used:

- A stainless steel jacket in which a sample of 7.8 cm in height and 3.8 cm in diameter was inserted with porous stones on top and bottom. The jacket was placed in a triaxial cell during saturation, so that to avoid vertical deformation. Saturation with deionised water was accomplished by applying injection pressures on top and bottom of 6 and 8 bar. Saturation was followed online by measurement of water intake through a volume change

apparatus. For the gas breakthrough test, the jacket on the base of the triaxial cell with the cell cap on top was placed in a frame to avoid vertical deformation of the bentonite (Figure 5). The test was performed in the modified setup described in section 3.1, in which the gas injection pressure on top was increased in 10-bar steps while backpressure at the bottom was atmospheric and the outflow was measured by a series of three different range on-line flowmeters. No bentonite vertical or lateral deformation was allowed but the mechanical stresses during saturation and breakthrough were not measured.

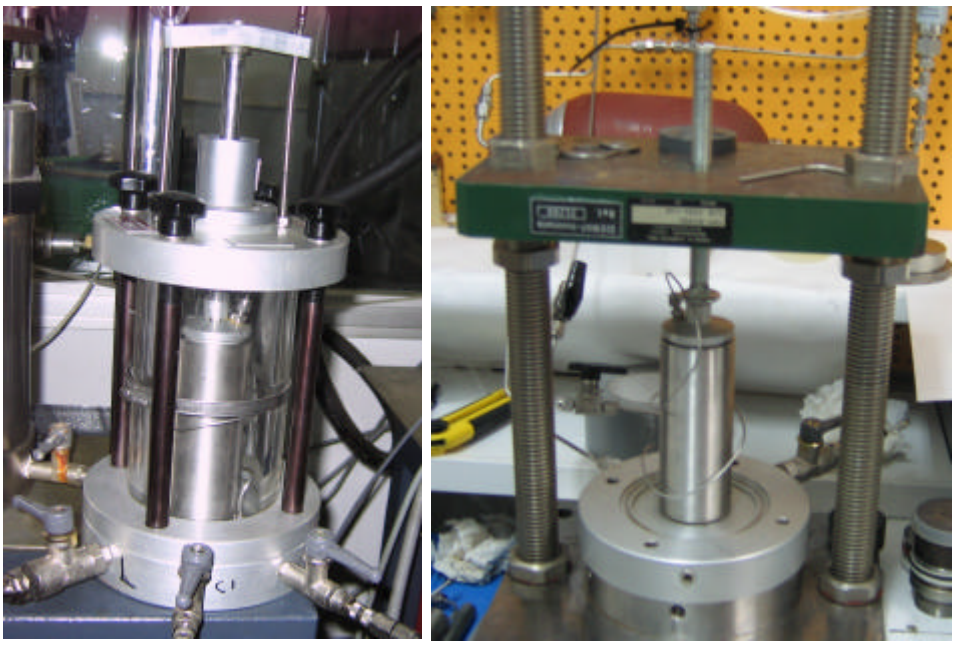

**Figure 5: Cell with stainless steel jacket for breakthrough tests: during saturation (left) and breakthrough measurement (right)**

- A series of stainless steel cells were designed and manufactured to perform gas breakthrough tests in saturated bentonite. The cells consisted of a body, in which the cylindrical sample was inserted, pistons with o-rings at both ends of the samples and threaded caps (Figure 6). The samples, of 3.8 and 5.0 cm in diameter and 5.0 in height, were obtained by uniaxial compaction of the bentonite with its hygroscopic water content directly inside the cell body. Saturation with deionised water was accomplished by applying an injection pressure of 6 bar to one end to allow air escaping from the bentonite. Later, the pressure was applied on top and bottom and, in the case of the higher density samples, increased progressively to 8 and 10 bar. In the higher density samples saturation was followed online by measurement of water intake through volume change apparatuses, whereas for lower density samples saturation was checked by weighing. Once saturated the filters on top and bottom of the samples were replaced by dry ones, the cells were again closed, and they were connected to a setup specially designed to measure breakthrough pressure (Figure 7). It consisted of two stainless steel deposits (SWAGELOK 304L-HDF4-75, SS Double-Ended DOT-Compliant Sample Cylinder, 75 $cm^3$, 124 bar) connected to the ends of the cell and pressurised with nitrogen gas at two different pressures. The pressures were measured by means of pressure transmitters DRUCK PMP 4070 (inlet pressure 135 bar a, outlet pressure 70 bar a, accuracy ±0.04% FS, over pressure 4 x FS). An HP 34970A data acquisition and switching mainframe, connected to a PC, recorded the data and monitored the tests in progress. If no changes in pressure were recorded during 24 h, the injection pressure was increased by 2 bar and kept constant for 24 h. The process was repeated until gas started to flow through the sample. The time required for the completion of a particular experiment was determined by the material and the conditions of the sample being studied.

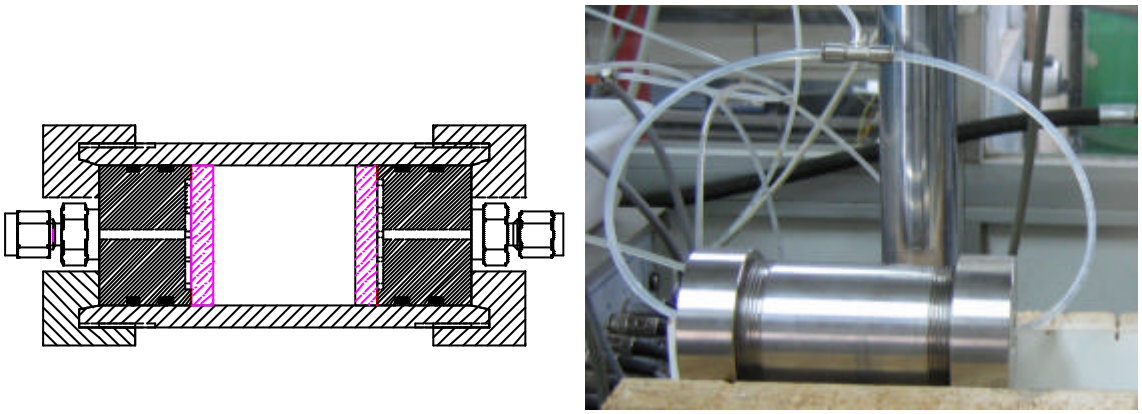

**Figure 6: Schematic cross-section and appearance of the breakthrough cells**

**Figure 7: Setup for measurement of breakthrough pressure in bentonite**

Although, these tests were not intended to measure permeability, after breakthrough in the setup just described, the flow of gas under the imposed pressure gradient could be measured from the decay of the pressure difference across the sample with elapsed time, as in a variable head permeameter. An indirect method was used to measure the volume flow rate entering in or coming from the sample (Loosveldt et al. 2002). The mean volume flow rate $Q_m$ was calculated as:

$$Q_m = V_v \times \left( \frac{\Delta r}{r} \right) \times \frac{1}{\Delta t} \qquad [3]$$

where $V_v$ is the volume of the deposit (inlet or outlet), $\Delta\rho/\rho$ is the relative change in gas density, and $\Delta_t$ is the time interval in which the change in gas density took place. To compute the change in gas density it has to be taken into account that, whereas the so-called permanent gases (those which are difficult to liquefy and have relatively low critical temperature) obey the ideal gas law to a satisfactory approximation, this is not the case at high pressure and low temperature. They are the so-called real gases and conform to the following equation:

$$P\,V = Z\,(P,T)\,n\,R\,T \qquad [4]$$

where $P$ is the absolute pressure (Pa), $V$ is the volume occupied by the gas ($m^3$), $n$ is the number of moles contained in volume $V$, $R$ is the ideal gas molar constant (8.3145 $J \cdot mol^{-1} \cdot K^{-1}$), $T$ is the absolute temperature (K) and $Z$ is the compressibility factor which depends simultaneously on

temperature and pressure. Hence, an ideal gas is by definition a gas with compressibility factor of 1. If $Z<1$, the gas is more compressible than the ideal gas taken in the same conditions of temperature and pressure, so that an identical volume will contain a larger quantity of gas. If $Z>1$, the gas is less compressible than the ideal gas taken in the same conditions of temperature and pressure, so that an identical volume will contain a lower quantity of gas. The density of the ideal gas ($\rho_{ideal}$) and the density of the supposedly ideal gas in identical conditions of temperature and pressure ($\rho^*$) are related through the expression:

$$Z = \frac{r_{ideal}}{r_{real}} = \frac{r^*}{r_{real}} \qquad [5]$$

The application of the ideal gas law immediately gives de value of $\rho^*$:

$$r^* = r_0 \frac{P}{P_0} \cdot \frac{T}{T_0} = \frac{M}{V_0} \cdot \frac{P}{P_0} \cdot \frac{T}{T_0} \qquad [6]$$

where $\rho_0$ is the density of the gas at reference conditions $T_0$ and $P_0$ (273.15 K and 101.325 kPa, STP), $V_0$ is the molar volume of the supposedly ideal gas at $T_0$ and $P_0$ (0.0224143 $m^3$/mol), $M$ is the molecular weight of the gas, $T$ and $P$ are the actual conditions.

Fluid physics equations and experimental observations have led to the determination of values of $Z$, which are listed in numerical tables (L'Air Liquide 1976). They show that the $Z$ value for nitrogen in the range of pressure and temperature of our tests corresponding to the maximal difference with respect to the ideal gas is 0.99364 ($N_2$ at 20°C and 48 bar-a). This $Z$ value indicates an underestimation of 0.64% in the actual density value when the gas is considered ideal and pressures are used to obtain the flow rate. However, the $Z$ value for nitrogen in the case of gas pressure of 200 bar-a (which was not actually reached in our tests) could cause an overestimation of the calculated permeability coefficients as high as 12% (at 25°C).

Note that when the actual densities deduced from Equation 5 are introduced in Equation 3, the compressibility factor $Z$ is eliminated from the equation. If the test is considered isothermal, then:

$$Q_m = V_v \times \left( \frac{\Delta P}{P_{av}} \right) \times \frac{1}{\Delta t} \qquad [7]$$

where $\Delta P$ is the pressure change and $P_{av}$ is the average pressure (upstream or downstream) in the deposit (inlet or outlet) during the time interval considered. The computation of permeability from the pressure decrease was performed then applying Equation 1, which became:

$$k_{ig} \cdot k_{rg} = [V_v]_{up,dw} \times \left( \frac{\Delta P}{P_{av}} \right)_{up,dw} \times \frac{1}{\Delta t} \times \frac{m_g \times L \times 2\, P_m}{A \times (P_{up}^2 - P_{dw}^2)} \qquad [8]$$

where $V_v$ is the volume of the upstream or downstream deposits, which is about 50 $cm^3$.

In this kind of tests the pressure of the measurement $P_m$ and the average pressure of the interval $P_{av}$ are coincident.

As in the constant pressure head tests, the accuracy of this analysis depends on the assumption that the gas behaved as an ideal gas and that a pseudo-steady state flow was established, *i.e.* that the quantity of gas exiting the high pressure vessel was approximately equal to that entering the low pressure vessel.

The permeability coefficient thus measured represents the sum of the permeability coefficient of the material and any additional contribution (cracks or incomplete sealing between sample and body cell). So the measured value would be higher than the permeability coefficient of the material and, therefore, the best value of the permeability coefficient of the material would be the lowest value obtained in a series of tests.

## 3.3 TESTS IN INTERFACES

These tests were carried out to check the gas transport performance of the interfaces between bentonite blocks and between bentonite and granite once the materials were saturated. Consequently, the first step was the preparation of the interfaces and their saturation.

### 3.3.1 Granite/bentonite interfaces

For the granite/bentonite interface two preliminary test were performed in a methacrylate cell (tests GB1 and GB2). A granite core of 5.2 cm in diameter and 6.6 cm in height was longitudinally cut in two halves, what resulted in rough granite surfaces. One of the halves was glued to a methacrylate cell with an epoxy adhesive (Figure 8, left). Additionally, three bentonite samples of 5.0 cm diameter and 2.2 cm height were obtained by uniaxial compaction of the clay. They were longitudinally cut in two halves using a Brazilian test apparatus. Those halves of the most appropriate size and consistency were stacked inside the methacrylate cell (Figure 8, right). Porous stones were placed on top and bottom and the cell was closed with stainless steel covers. Saturation proceeded from the bottom with deionised water, initially under a low pressure. Once saturated the cell GB1 was dismounted and weighed, to check the final bentonite water content, the porous filters were replaced by dry ones, and the cell was closed again. The sample was tested for gas breakthrough in the modified setup described in section 3.1 (Figure 9). A nitrogen gas pressure of 2 bar was applied on top of the sample and increased in 1-bar steps until breakthrough was reached.

The 5-cm internal diameter cells described in the previous section (Figure 6) were also used for the granite/bentonite interface tests. The samples were prepared following the same procedure as for the methacrylate cell and they are currently saturating with deionised water injected at a pressure of 0.05 bar. In test GB3 the bentonite was initially compacted with its hygroscopic water content at a dry density of 1.6 g/cm$^3$ and in test GB4 at a dry density of 1.8 g/cm$^3$.

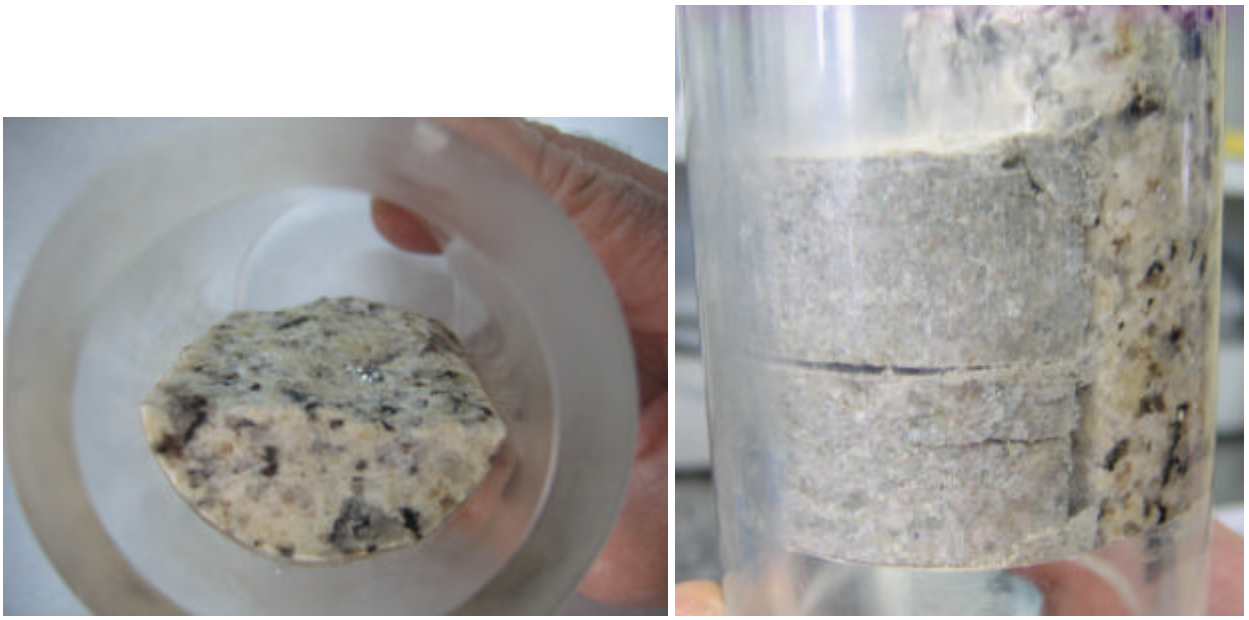

**Figure 8: Preparation of the preliminary test for granite/bentonite interface GB2**

**Figure 9: Methacrylate cell during the granite/bentonite interface gas breakthrough test GB1**

### 3.3.2 Bentonite/bentonite interfaces

The samples for tests on bentonite blocks interfaces were prepared by uniaxially compacting cylindrical specimens that were later longitudinally cut with a saw (Figure 10). The clay was used with its hygroscopic water content and compacted to dry densities of 1.7 and 1.8 g/cm$^3$. After cutting the cylinders, the halves were put together inside stainless steel cells of 3.8 cm internal diameter and 5 cm height (Figure 6) with geotextile on top and bottom. The cutting process implied mass loss, and consequently a reduction in dry density to values of 1.48 and 1.68 g/cm$^3$. Saturation took place with deionised water through both ends under an injection pressure of 0.2 MPa during 25 days and then under an injection pressure of 0.6 MPa.

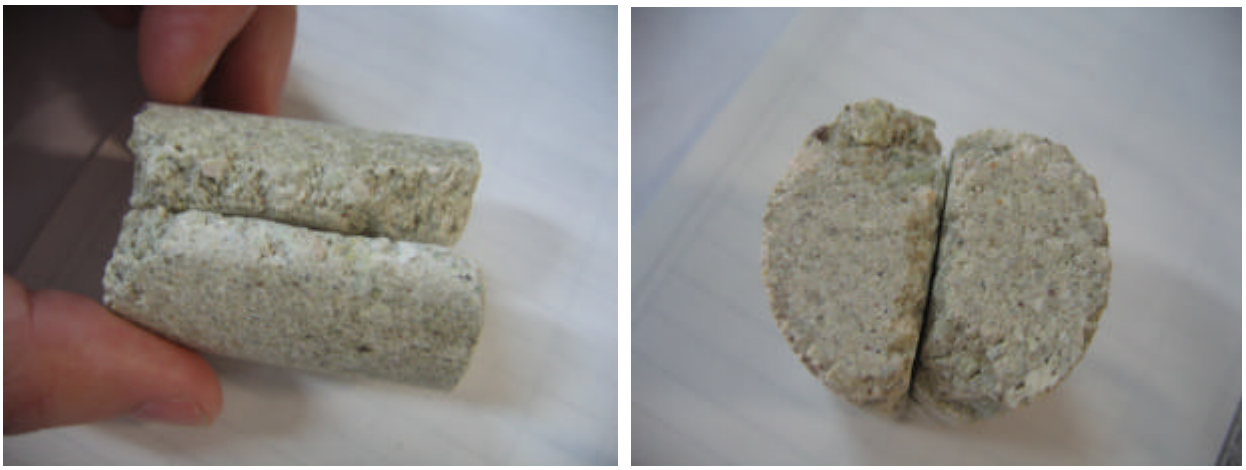

**Figure 10: Appearance of a sample for bentonite interfaces testing**

# 4 Results

## 4.1 GAS PERMEABILITY

Gas permeability was measured in samples compacted at dry densities of between 1.4 and 1.8 g/cm$^3$ with water contents between 18 and 22%, corresponding to initial degrees of saturation between 62 and 97%. The gas pressures applied during the tests were those shown in Figure 3, with a maximum injection pressure of 8 bar and a maximum confining pressure of 10 bar, which was well below the expected swelling pressure. It was checked that for a given sample and test step the gas outflow was equal to the gas inflow, and thus the intrinsic permeability calculated was the same despite the flow (in or out) used to compute it. However, when gas permeability was calculated taking into account the fluid properties (*i.e.* the permeability in m/s), the gas permeability upstream was usually slightly higher than downstream, up to a maximum of one order of magnitude when the upstream and downstream pressures were very different. This was due to the variation of the fluid properties with pressure and gives an idea of the possible range of variation of gas permeability inside the sample due to the gas pressure gradient.

A summary of the characteristics of the tests performed is given in Table I, where the initial and final dry density ($\rho_d$), water content ($w$), degree of saturation ($S_r$) and accessible void ratio ($e(1-S_r)$) are shown, along with the average permeability value obtained with the gas outflow for all the steps in which backpressure was atmospheric. The differences between the initial and final conditions were due to progressive decompression of the samples (since they were compacted applying very high pressures). Final checking of water content at different levels showed that the differences in water content along the samples were smaller than 0.4%, with a trend to find lower water contents towards the end of the sample where gas injection was applied (on top).

These values are plotted in Figure 11 grouped by the initial water content. The decrease of gas permeability with dry density was substantial, several orders of magnitude for an increase of dry density from 1.5 to 1.8 g/cm$^3$. The effect of water content was not very noticeable due to the fact that the range tested was not broad, however, higher water content samples tended to have lower permeabilities. In fact, the samples could be separated in two widespan groups: those with water contents around 18% and those with water contents around 20%, which is the separation considered in the rest of the report.

**Table I: Summary of the gas permeability tests performed**

| Reference | Initial $\rho_d$ (g/cm$^3$) | Initial $w$ (%) | Initial $S_r$ (%) | Final $\rho_d$ (g/cm$^3$) | Final $w$ (%) | Final $S_r$ (%) | $e(1-S_r)$ | $k_g$ (m/s) | $k_{ig} \cdot k_{rg}$ (m$^2$) |
|---|---|---|---|---|---|---|---|---|---|
| PGFBX1 | 1.51 | 13.1 | 45 | | 14.1 | 48 | 0.43 | $7.3 \cdot 10^{-9}$ | $1.1 \cdot 10^{-13}$ |
| PGFBX2 | 1.40 | 21.3 | 62 | | 21.4 | 62 | 0.36 | $8.8 \cdot 10^{-8}$ | $8.6 \cdot 10^{-14}$ |
| PGFBX3 | 1.68 | 18.2 | 81 | 1.68 | 16.7 | 74 | 0.11 | $1.4 \cdot 10^{-9}$ | $2.0 \cdot 10^{-15}$ |
| PGFBX4 | 1.76 | 18.4 | 93 | 1.73 | 17.7 | 89 | 0.04 | $1.2 \cdot 10^{-10}$ | $1.7 \cdot 10^{-16}$ |
| PGFBX5 | 1.80 | 17.7 | 96 | 1.73 | 19.4 | 93 | 0.02 | $2.3 \cdot 10^{-12}$ | $3.4 \cdot 10^{-18}$ |
| PGFBX6 | 1.78 | 18.6 | 97 | 1.74 | 18.9 | 93 | 0.01 | $4.7 \cdot 10^{-12}$ | $7.0 \cdot 10^{-18}$ |
| PGFBX7 | 1.76 | 17.8 | 90 | 1.72 | 18.1 | 86 | 0.05 | $4.2 \cdot 10^{-11}$ | $6.2 \cdot 10^{-17}$ |
| PGFBX8 | 1.78 | 18.1 | 94 | 1.72 | 19.3 | 91 | 0.03 | $2.2 \cdot 10^{-12}$ | $3.4 \cdot 10^{-18}$ |
| PGFBX9 | 1.76 | 19.0 | 96 | 1.71 | 19.9 | 92 | 0.02 | $5.5 \cdot 10^{-12}$ | $8.3 \cdot 10^{-18}$ |
| PGFBX10 | 1.62 | 22.7 | 92 | 1.55 | 22.1 | 80 | 0.06 | $3.4 \cdot 10^{-9}$ | $4.7 \cdot 10^{-15}$ |
| PGFBX11 | 1.65 | 18.4 | 78 | 1.62 | 17.9 | 73 | 0.14 | $1.5 \cdot 10^{-9}$ | $2.3 \cdot 10^{-15}$ |
| PGFBX12 | 1.70 | 18.3 | 85 | 1.68 | 18.4 | 81 | 0.09 | $1.9 \cdot 10^{-10}$ | $2.8 \cdot 10^{-16}$ |
| PGFBX13 | 1.76 | 17.6 | 89 | 1.73 | 17.7 | 85 | 0.06 | $2.3 \cdot 10^{-11}$ | $3.6 \cdot 10^{-17}$ |
| PGFBX14 | 1.78 | 18.5 | 97 | 1.72 | 19.7 | 93 | 0.02 | $8.4 \cdot 10^{-12}$ | $1.3 \cdot 10^{-17}$ |
| PGFBX16 | 1.78 | 18.7 | 97 | 1.61 | 21.4 | 85 | 0.01 | $1.1 \cdot 10^{-13}$ | $1.9 \cdot 10^{-19}$ |

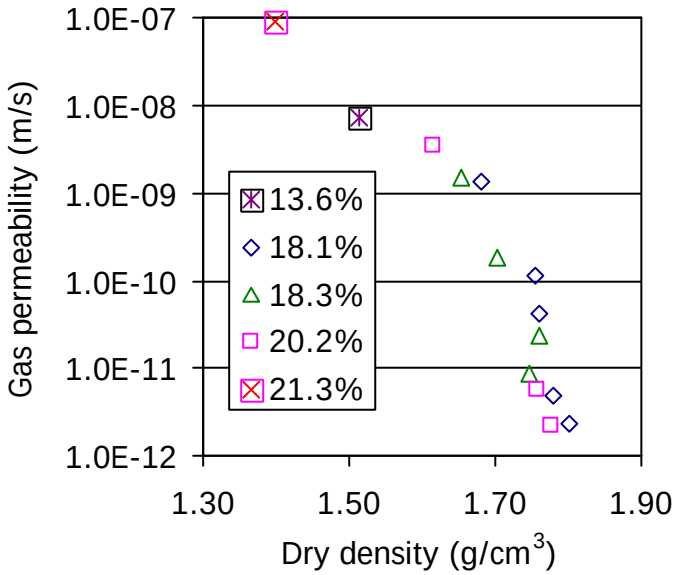


**Figure 11: Average gas permeability (shown in Table I) for different water contents as a function of bentonite dry density**

The permeability values obtained during Stage 1 (Figure 3) are plotted in Figure 12. The effect of dry density, and particularly degree of saturation, on gas permeability was very clear, both for the samples with water content 18% and 20%. The same comment could be made for the values obtained during Stage 3 (Figure 13), in which the confining pressure was 10 bar instead of 6 bar. For the samples with water content 20%, the increase in the degree of saturation from 80 to 90% gave place to a decrease in permeability of three orders of magnitude. In the range of pressures tested, no effect of the injection pressure on the permeability value obtained was observed.

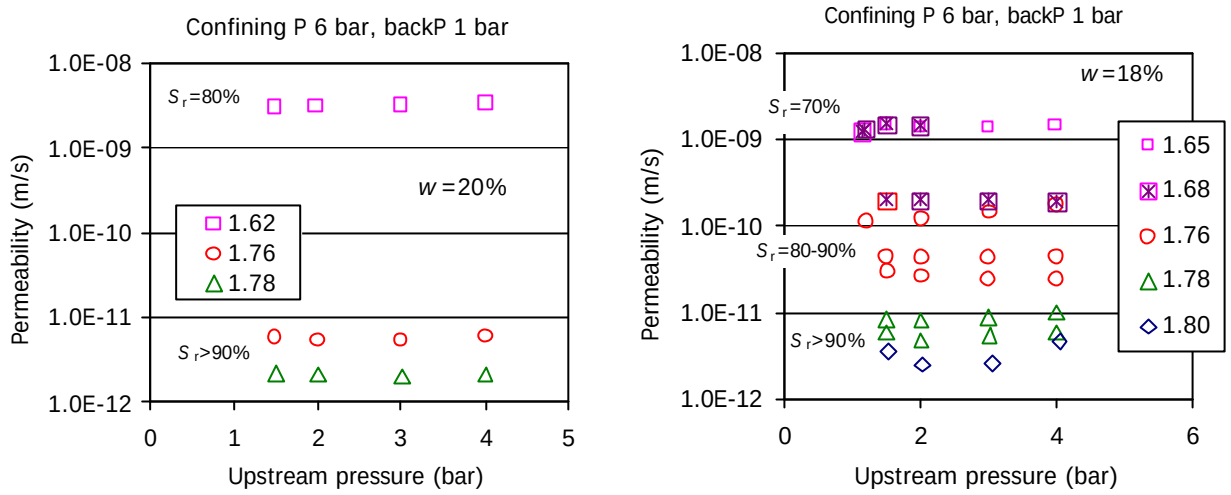


**Figure 12: Gas permeability measured during Stage 1 for samples of average water content 20% (left) and 18% (right). The dry density of the samples is indicated in the legends in g/cm$^3$**

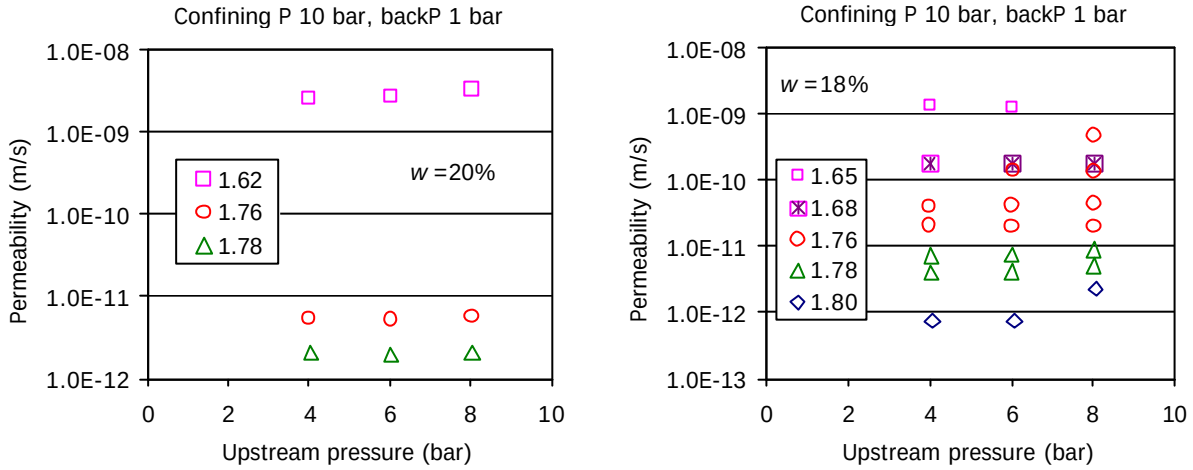


**Figure 13: Gas permeability measured during Stage 3 for samples of average water content 20% (left) and 18% (right). The dry density of the samples is indicated in the legends in g/cm$^3$**

The effect of the confining pressure on permeability was checked during Stage 2, in which the confining pressure was increased from 6 to 10 bar, while the injection and backpressure were constant (Figure 14). In test FBX14 the confining pressure was increased up to 12 bar. For the range of pressures tested in this series of tests, the confining pressure did not affect the permeability value. Test FBX16 was performed in a cell that allowed the application of higher confining and injection pressures, since the initial degree of saturation was very high (97%) and the permeability expected very low. The pressure path followed in this test is shown in Figure 4. It was observed that each time the confining pressure was increased, the permeability value decreased slightly (Figure 15). This decrease could be attributed to the increase in effective pressure resulting from the confining pressure increase while injection pressure was unchanged. In fact, for each confining pressure, as the injection pressure was increased, the permeability value increased also, due to the decrease in effective pressure. In any case, the changes observed are small.

Since the initial degree of saturation of tests FBX14 and FBX16 were the same, the permeability values, which were obtained under very different pressure conditions (low for test FBX14 and

high for test FBX16), can be compared (Figure 16). Gas permeability tended to decrease with the increase in effective pressure, without major changes as confining pressure was varied. However, the change from the low to the high range of confining (and consequently effective) pressure, did imply an almost 2-order of magnitude decrease in gas permeability.

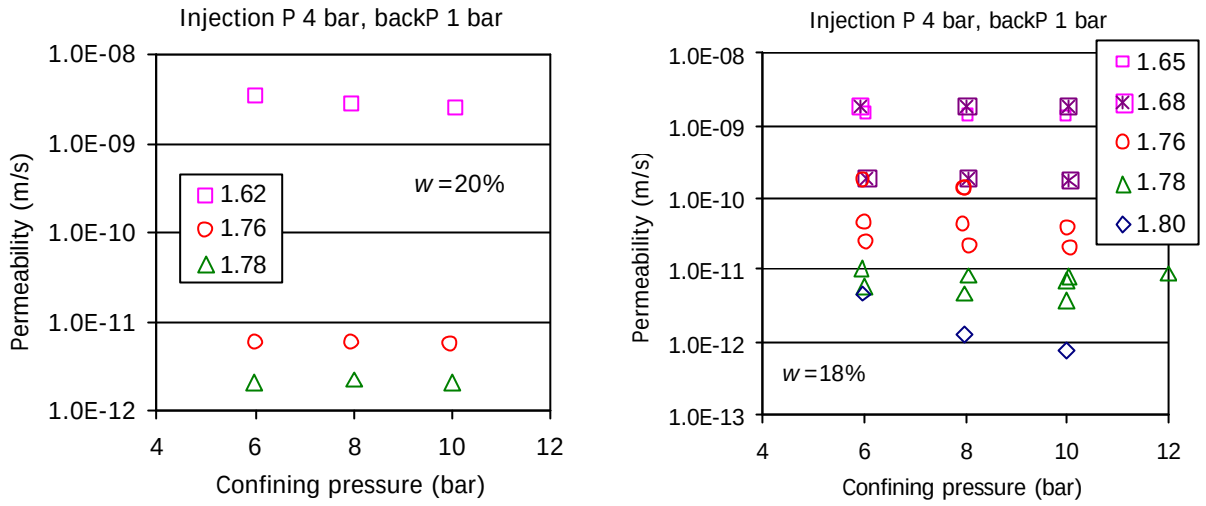


**Figure 14: Effect of confining pressure on gas permeability measured during Stage 2 for samples of average water content 20% (left) and 18% (right). The dry density of the samples is indicated in the legends in g/cm$^3$**

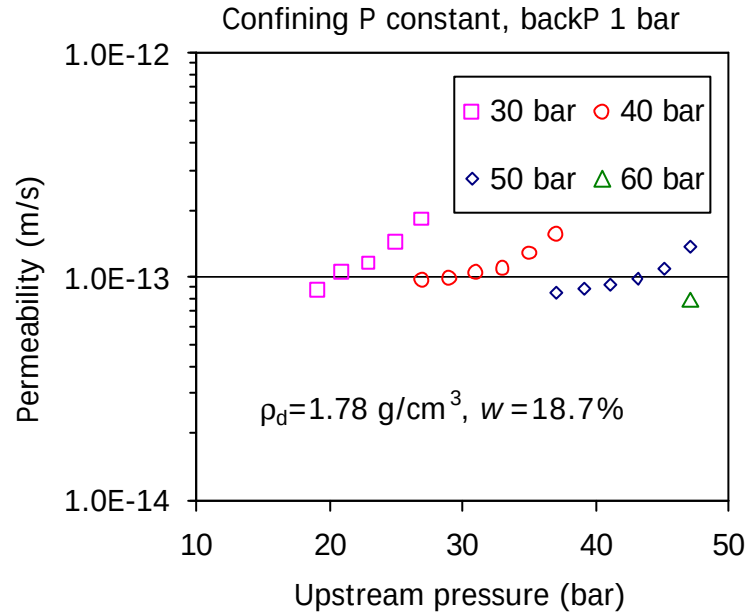


**Figure 15: Gas permeability measured in test FBX16 (initial $S_r$=97%) for different confining pressures (indicated in the legend)**

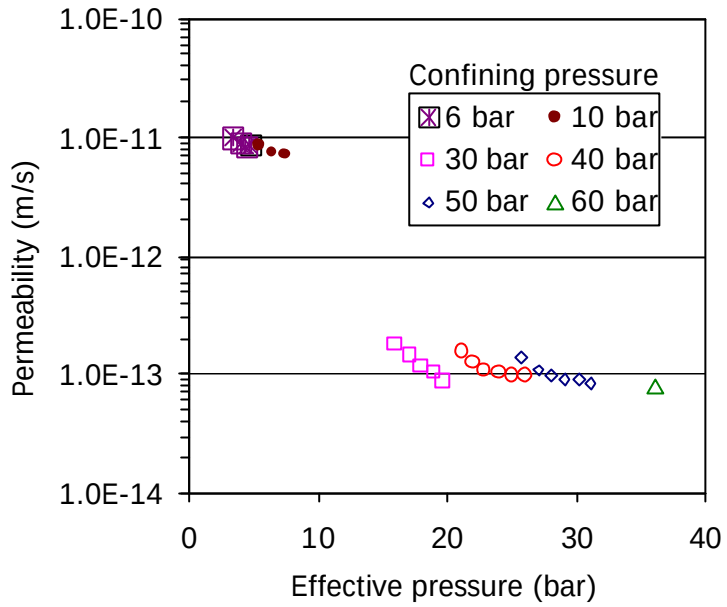


**Figure 16: Comparison of gas permeability obtained in tests FBX14 and FBX16 (initial $S_r$=97%) for different effective pressures. Backpressure was atmospheric**

The effect of backpressure on permeability was tested during Stage 4 and 5 of the tests (Figure 3). The gas permeability values obtained during these stages are shown in Figure 17. The increase in backpressure implied a decrease in effective pressure and consequently an increase in gas permeability.

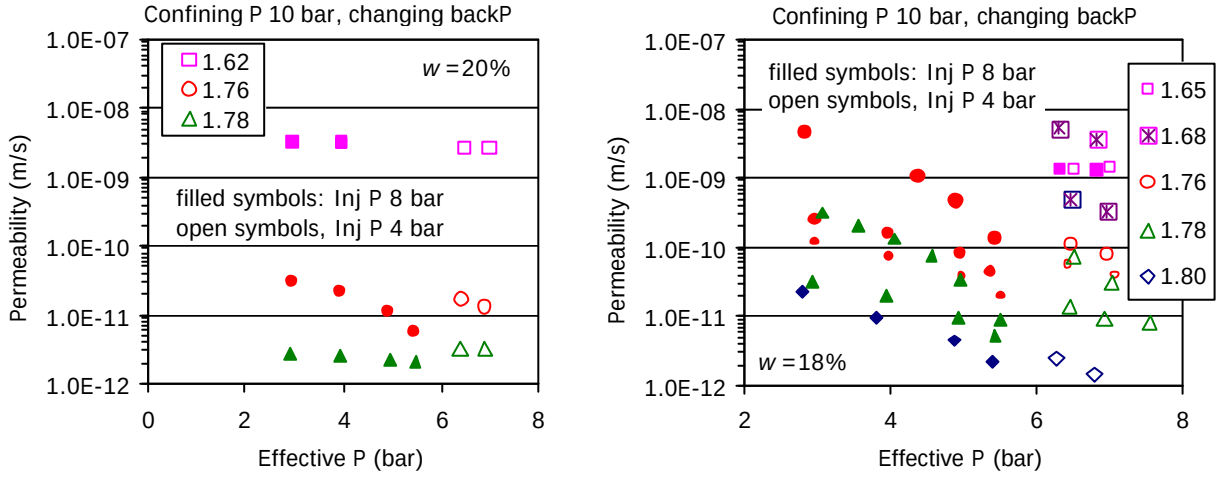


**Figure 17: Effect of effective pressure on gas permeability measured during Stages 4 and 5 for samples of average water content 20% (left) and 18% (right). The dry density of the samples is indicated in the legend in g/cm$^3$**

## 4.2 BREAKTHROUGH TESTS

A sample of 7.8 cm in height and 3.8 cm in diameter was saturated with deionised water inside a stainless steel jacket by applying injection pressures on top and bottom of 6 bar for 225 days. The initial dry density and water content of the sample were 20% and 1.73 g/cm$^3$, respectively. The water content at the end of the saturation phase was 28.2%, and the density could have slightly decreased, due to the small vertical deformation allowed.

For the gas breakthrough test the jacket with the sample inside was placed in a frame to avoid vertical deformation of the bentonite (Figure 5). The gas injection pressure on top was

increased from 22 to 100 bar in 10-bar steps while backpressure at the bottom was atmospheric. Each step was held for between 24 and 72 h. No outflow was recorded in any of the steps. The upper limit of the equipment was 100 bar, and this pressure was kept for more than 30 days without any outflow or pressure decrease being recorded.

In addition, a series of stainless steel cells were used to perform gas breakthrough tests in saturated bentonite (Figure 6). The bentonite was compacted with its hygroscopic water content to dry density of 1.4 and 1.5 g/cm$^3$. Saturation with deionised water was accomplished by applying injection pressures on top and bottom of 6 (for dry density 1.4 g/cm$^3$) or 10 bar (for dry density 1.5 g/cm$^3$). Two cells with bentonite samples compacted at dry density 1.4 g/cm$^3$ were considered saturated after 80 days (tests BT1.4_1 and BT1.4_2). They were connected to the setup to measure breakthrough pressure (Figure 7). An initial pressure of 10 bar was fixed in the inlet deposits, while a vacuum of 260 mbar-a was applied to the outlet deposits.

For the sample in the 38-mm diameter cell (test BT1.4_1) the upstream pressure was increased by 2 bar and kept constant for at least 24 h. This process was repeated until the injection pressure reached a value of 52 bar. The evolution of pressure in the upstream and downstream deposits is shown in Figure 18. The pressure in the outlet deposit slightly increased from the beginning of the test, what could be explained by the evaporation of the water displaced (the equilibrium water vapour pressure at 25°C is approximately 3167 Pa). When the injection pressure was increased to 52 bar, the pressure in the inlet deposit started to decrease while that in the outlet deposit increased, what indicated the occurrence of breakthrough.

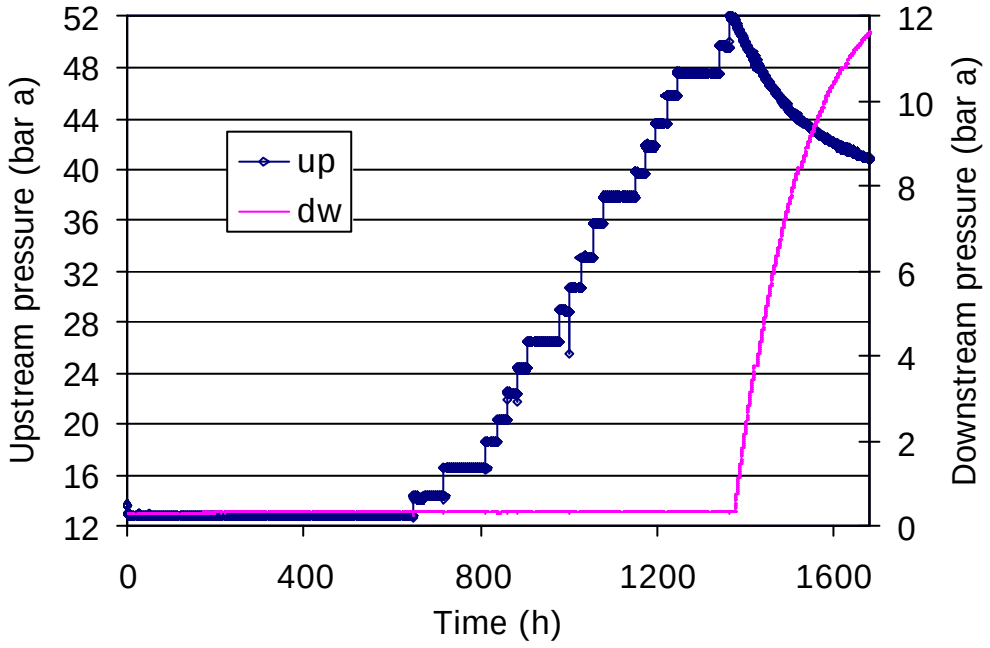


**Figure 18: Gas pressure evolution in the inlet and outlet deposits of gas breakthrough test BT1.4_1 (diameter 38 mm)**

However, the sample in the 50-mm diameter cell (test BT1.4_2) recorded an inlet pressure decrease from the beginning of the test, *i.e.* for an injection pressure of 10 bar. After 60 min (flight time) a linear downstream increase was recorded (Figure 19**)**, what clearly indicated steady gas flow through the bentonite. When the pressure is plotted taking this moment as time 0, the pressure change in both deposits is perfectly symmetrical (Figure 20), considering that nitrogen behaves as an ideal gas for this range of pressures. From the pressure change, and taking into account the deposits' volume, the flow can be computed and consequently the permeability (Equation 8). The values thus computed are plotted in Figure 21. After 64 days the

cell was dismounted, weighed and subjected to resaturation with deionised water under an injection pressure of 8 bar.

The different behaviour of tests BT1.4_1 and BT1.4_2, despite the fact that the nominal dry density of the bentonite in both cases was the same (1.4 g/cm$^3$), points to an actual difference of the bentonite density between both tests, which would be due to a mistake during manufacturing of the samples. This will be checked at the end of the tests.

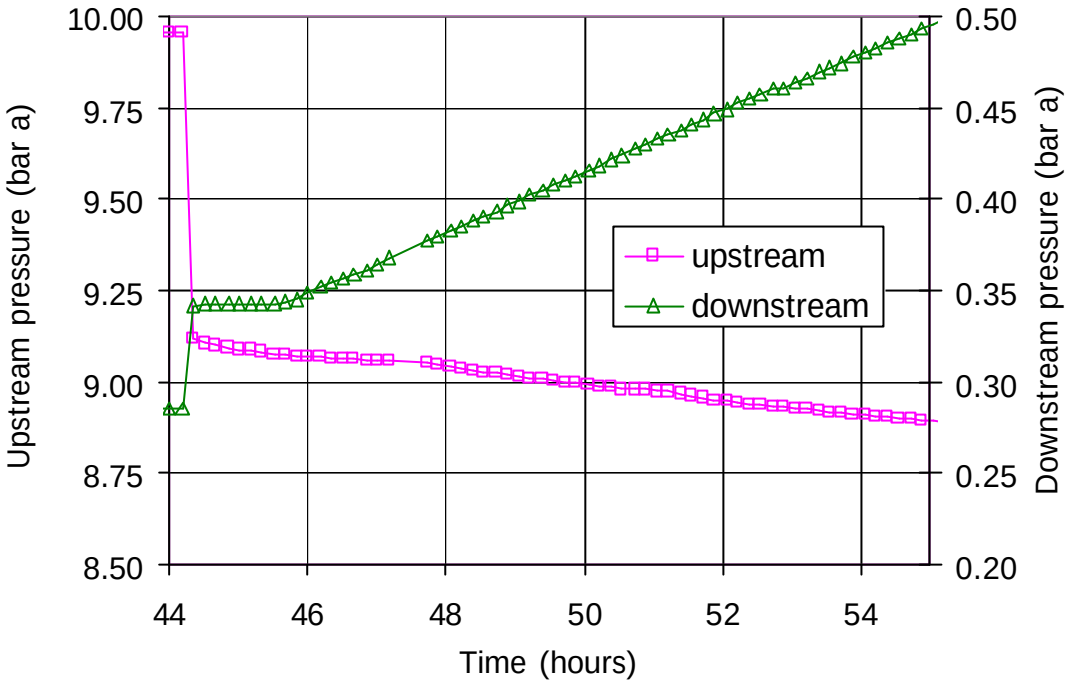


**Figure 19: Gas pressure evolution in the inlet and outlet deposits of test BT1.4_2 (diameter 50 mm) at the beginning of the test (t=0 is the time from the beginning of the experiment)**

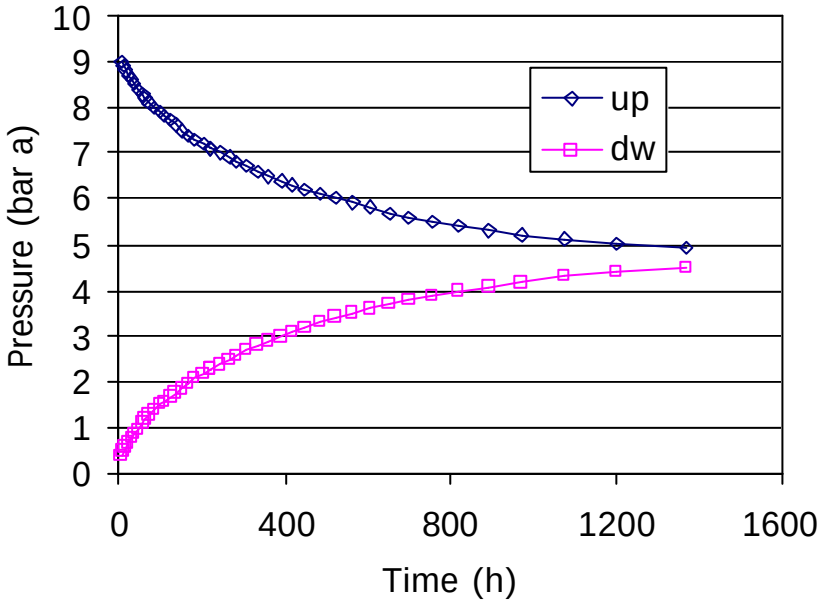


**Figure 20: Gas pressure evolution in the upstream (up) and downstream (dw) deposits of test BT1.4_2 (diameter 50 mm). The initial delay in the response of the outlet deposit was corrected (t=0 is the time after steady state flow)**

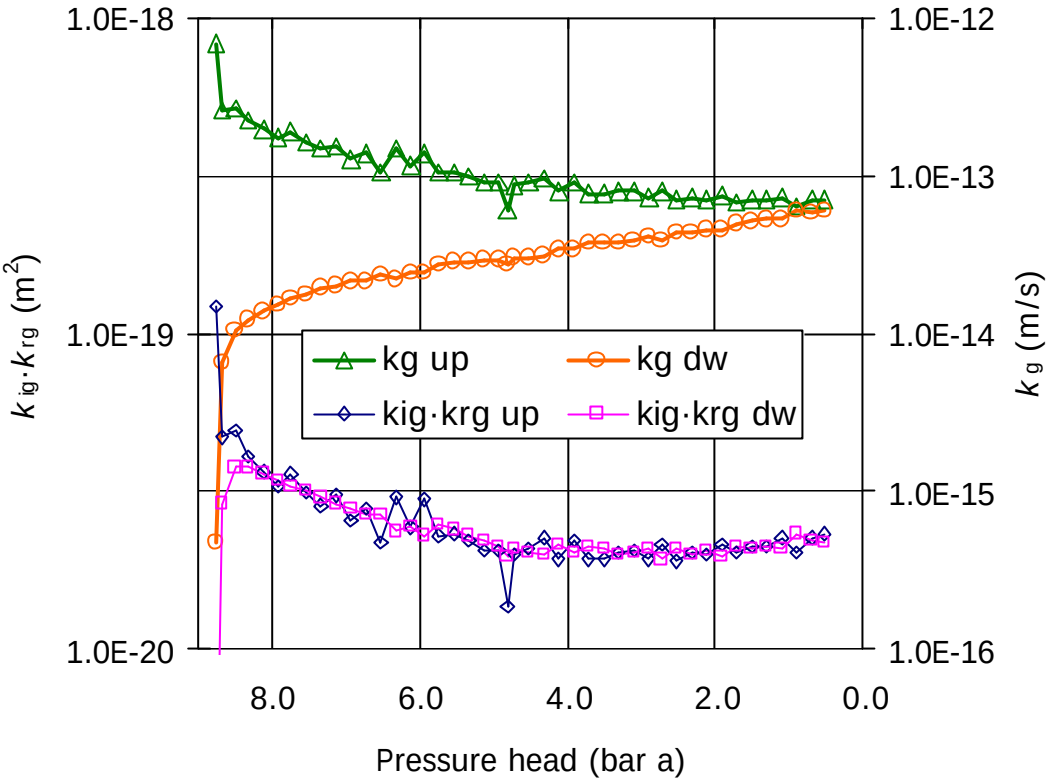


**Figure 21: Average gas permeability values computed from the pressure measurements in the upstream (up) and downstream (dw) deposits in test BT1.4_2 with Equation 8**

## 4.3 TESTS IN INTERFACES

### 4.3.1 Granite/bentonite interfaces

The preliminary test GB1 was carried out according to the procedure described in section 3.3.1. The dry density of the bentonite inside the cell was 1.56 g/cm$^3$. The bentonite had initially a water content of 17% and after saturation for 181 days, under a very low pressure (a 21-cm water column) for the first 69 days and under a pressure of 0.2 MPa afterwards, the water content was of 31.1%. The progress of saturation can be seen in Figure 22.

The cell was then dismounted to change the porous filters by dry ones and a gas breakthrough test started in the modified setup described in section 3.1. A nitrogen gas pressure of 2 bar was initially applied on the top surface, while the pressure at the bottom was atmospheric. The gas outflow was continuously monitored. Afterwards, the injection pressure was increased in 1-bar steps according to the sequence shown in Figure 23. No gas outflow or pressure decrease was observed until the injection pressure reached 7 bar. Then the gas outflow increased as the injection pressure decreased, indicating the breakthrough of the interface (Figure 24). The outflow stopped because the gas deposit was exhausted. After a few hours the test was restarted and breakthrough took place for an injection pressure of 3 bar. The water content at the end of the test was 29.7%, and the drying along the interface was clearly visible.

After this gas breakthrough test the cell was resaturated through the bottom surface under a low water pressure (21-cm high column) for 50 days and tested again for gas breakthrough following a pressure path similar to that shown in Figure 23. For a second time breakthrough took place for an injection pressure of 7 bar (Figure 25). After breakthrough the air flowed through the sample for 48 h, what caused drying of the sample to an average water content of 21.1%. This flow took place under an average hydraulic head of 0.1 bar, and the permeability

computed from it considering that flow took place through the bentonite surface was $1.2 \cdot 10^{-8}$ m/s. However, the flow probably occurred along the fracture. In fact, upon dismantling it was observed that the interface between the bentonite and the granite was particularly dry and the bentonite had slightly retracted along it (Figure 26). The water content of the ends of the sample was considerably lower than in the central part, particularly in the end through which gas injection took place, which was also the part of the column farthest from the hydration surface.

Another sample was prepared following the same procedure but with a higher bentonite density (test GB2). The bentonite blocks were initially compacted at a dry density of 1.90 g/cm$^3$, although the density of the bentonite inside the cell, once all the voids filled, was 1.83 g/cm$^3$. After 9 days of saturation under a very low pressure (a 21-cm water column), the methacrylate broke and the test had to be suspended.

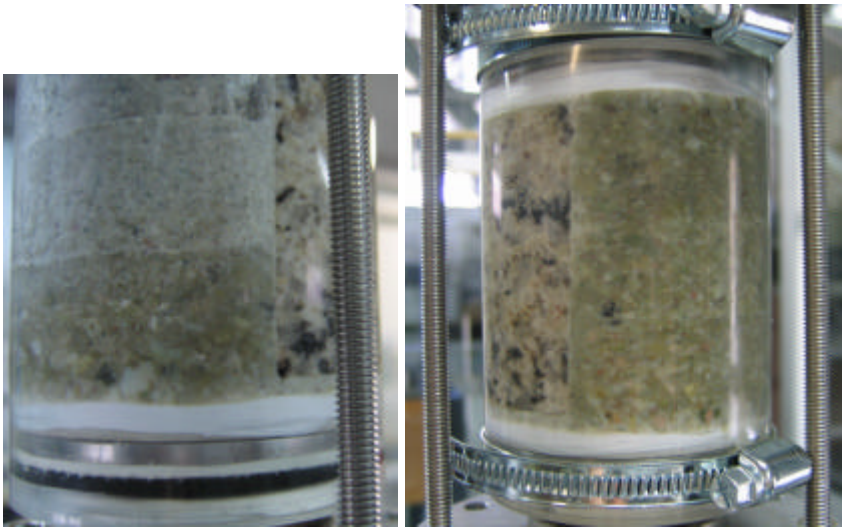

**Figure 22: Evolution of saturation in the granite/bentonite interface test GB1 (12 days, left; 153 days, right)**

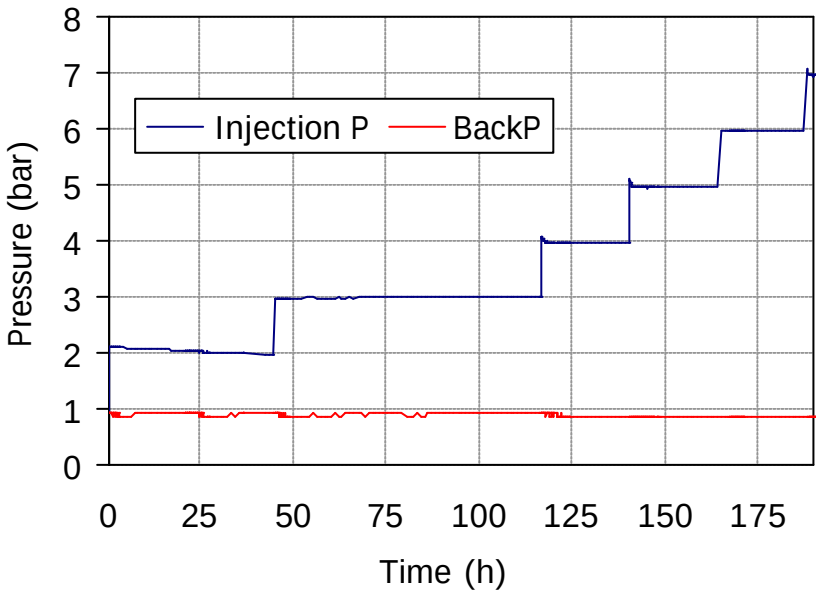


**Figure 23: Pressure path followed in the granite/bentonite interface test GB1**

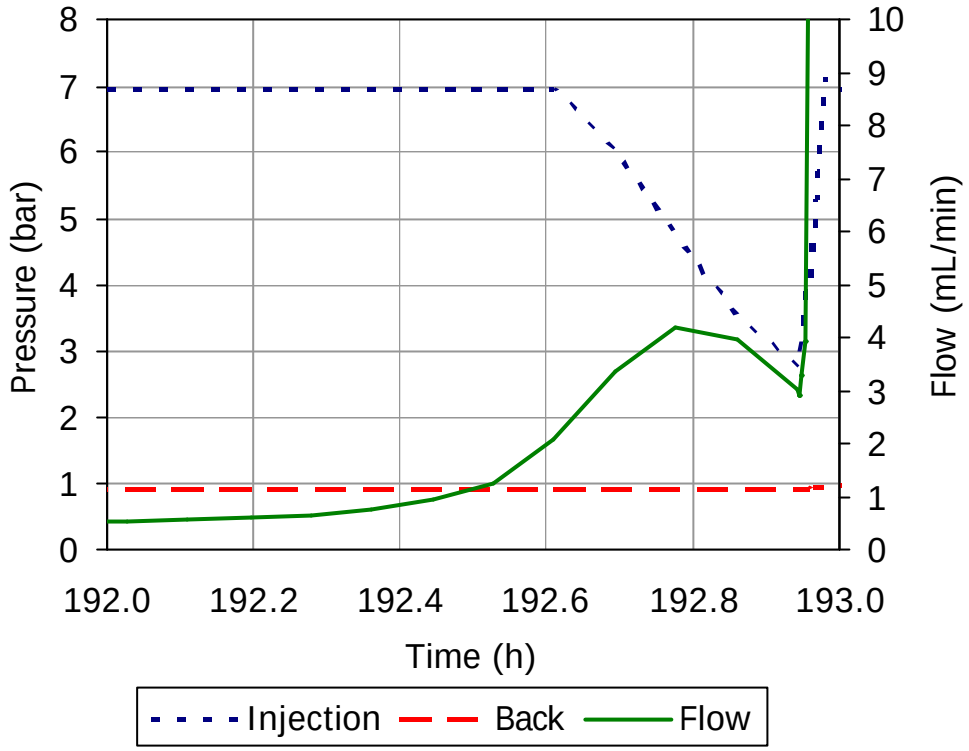


**Figure 24: Breakthrough measurement in the granite/bentonite interface test GB1**

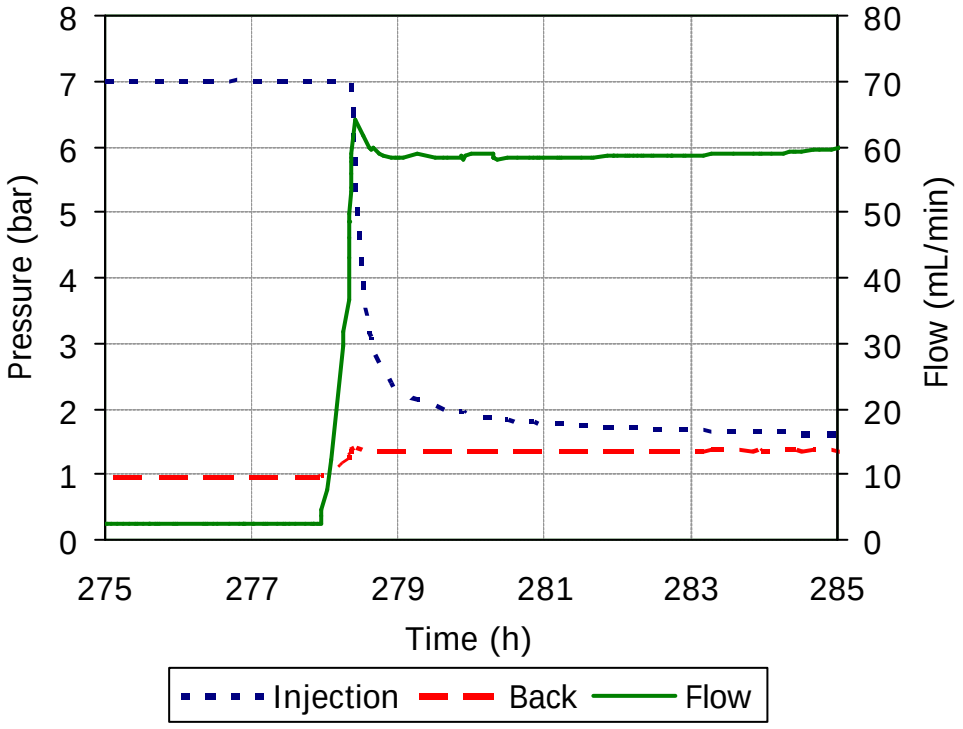


**Figure 25: Second breakthrough measurement (after resaturation) in the granite/bentonite interface test GB1**

**Figure 26: Appearance of the granite/bentonite interface after the second gas breakthrough in test GB1**

### 4.3.2 Bentonite/bentonite interfaces

Two bentonite/bentonite interface samples were prepared according to the procedure described in section 3.3.2. Both are currently saturating, and the evolution of their water content is shown in Figure 27.

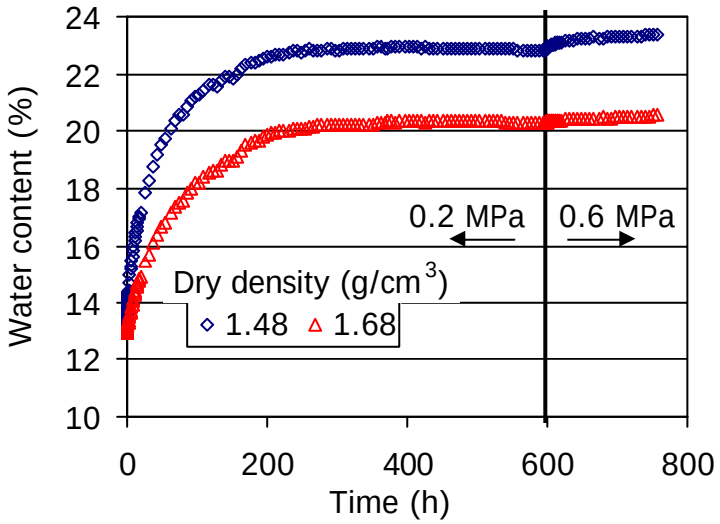


**Figure 27: Water content evolution during saturation of two bentonite/bentonite interface tests**

# 5 Discussion

It is acknowledged that at low gas pressures there can be very few molecules of gas occupying some of the smaller pores, what would lead to an overestimation in the permeability known as the gas slippage or the Klinkenberg effect. It is corrected for by making permeability measurements with gas at multiple pressure differences and constructing a graph of the

measured apparent permeability ($k_{ig}$·$k_{rg}$) against the reciprocal of the mean pressure in the samples. The mean pressure ($P_m$) is the average of the upstream ($P_{up}$) and downstream ($P_{dw}$) pressures in Equation 1. This was done for several of the tests presented above and the result is shown in Figure 28. The points should lie on a straight line which intersects the *y*-axis at $1/P_{mn}$ = 0. This value effectively represents the permeability at which the gas is compressed by infinite pressure and becomes a near perfect liquid. The values obtained in the graph were only slightly smaller (by a factor of 1.1 to 1.3) than the values measured and shown in Table I, for which reason it was considered that the Klinkenberg effect was not relevant in the range of pressures applied and the values obtained were not corrected for.

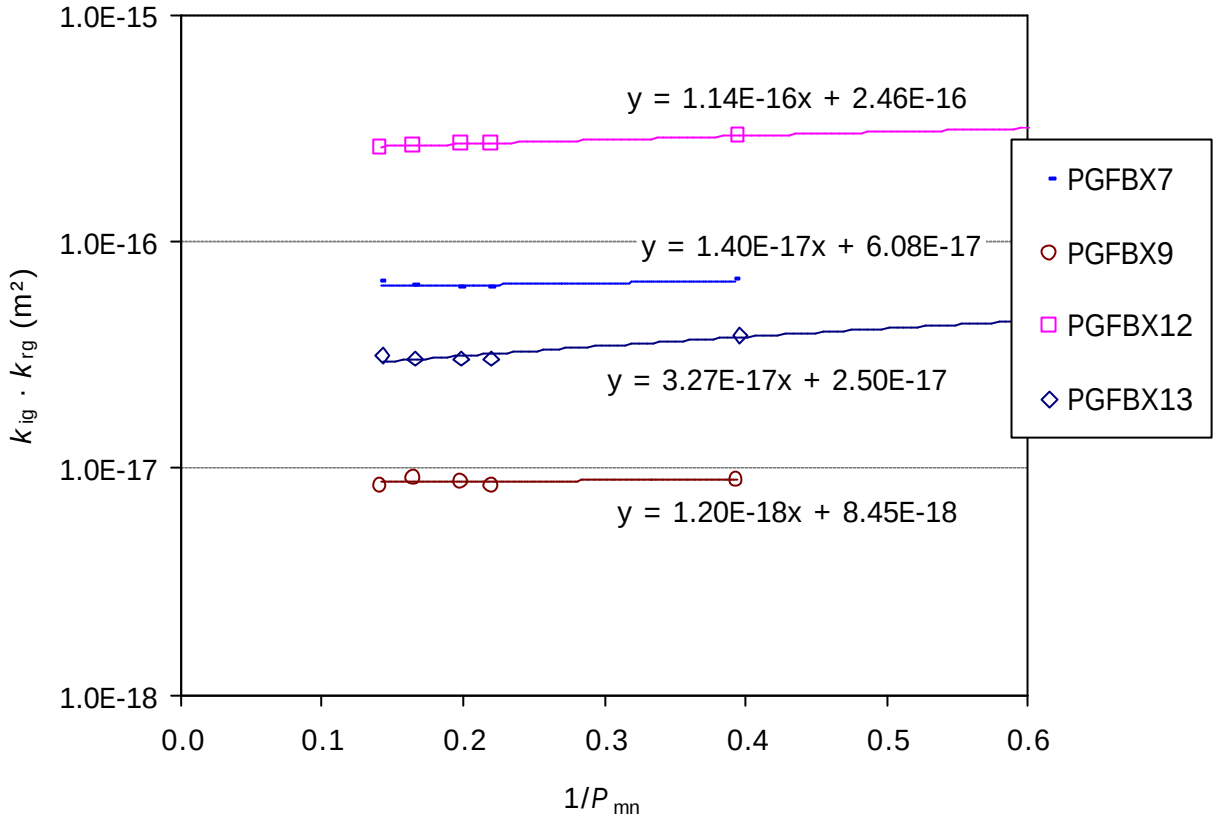


**Figure 28: Klinkenberg correction plot for some of the tests performed. Only the steps of the tests in which the hydraulic head was 2 bar (Figure 3) were taken into account**

Some years ago, during the FEBEX project, the gas permeability of samples of FEBEX bentonite compacted to different dry densities with different water contents was measured in a falling head permeameter under gas injection pressures just slightly above atmospheric, thus much lower than those used for the samples tested in FORGE. It was found that the gas permeability ($k_g$, in m/s) was best correlated to the accessible porosity through the following empirical correlation (Villar 2002):

$$k_g = 2.3 \cdot 10^{-6} \, (e(1-S_r))^{4.17} \qquad [9]$$

where *e* is the void ratio and $S_r$ is the degree of saturation in percentage. Those results are plotted in Figure 29, in which the new results have also been plotted (Table I). The samples tested during FEBEX had lower degrees of saturation than those tested in FORGE, because the low injection pressures applied then did not allow for gas flow under high degrees of saturation. The new results obtained with highly saturated samples agree with those obtained in less saturated samples and with low injection pressure during FEBEX, and all of them fit in the new correlation shown in the Figure. A similar correlation can be found for the $k_{ig}$·$k_{rg}$ value:

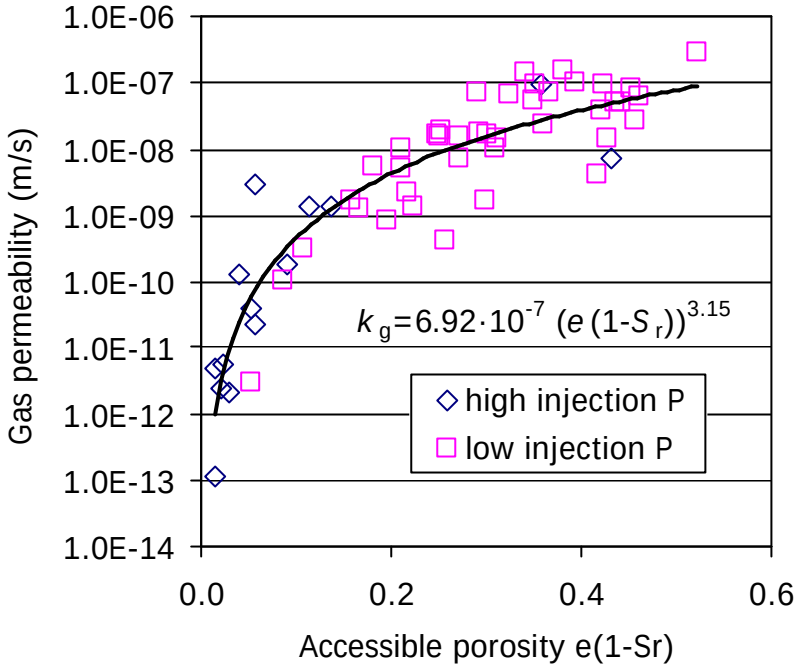


**Figure 29: Gas permeability as a function of the accessible porosity for FEBEX samples tested during the FEBEX (low injection P) and the FORGE (high injection P) projects**

$$k_{ig} \cdot k_{rg} = 1.25 \cdot 10^{-12} (e(1-S_r))^{3.22} \quad [10]$$

If we made the degree of saturation 0 in Equation 10, we would obtain the intrinsic permeability value as a function of void ratio for the dry bentonite ($k_{ig}$), since the relative permeability to gas ($k_{rg}$) in a dry sample would be 1:

$$k_{ig} = 1.25 \cdot 10^{-12} e^{3.22} \quad [11]$$

These values cannot be actually measured, because the drying of the bentonite to such low degree of saturation would imply the modification of its microstructure by shrinkage. During FEBEX it was demonstrated that these intrinsic permeability values are much higher (up to 8 orders of magnitude) than those found for the saturated bentonite using water as permeating fluid, since the pore size distribution is greatly modified during hydration (Villar 2002, Villar & Lloret 2001).

The intrinsic permeability values thus obtained were introduced in Equation 1 for each test (last column in Table I) and then the relative permeability value for each sample tested, of a given *e*, was obtained. The values thus computed are plotted in Figure 30 as a function of the void ratio. They are very low because the degrees of saturation of the samples were very high, and it was found during FEBEX that the decrease of gas permeability for degrees of water saturation higher than a threshold value (between 65 and 80%, depending on the dry density) was very sharp, due to the discontinuity of the gas phase (Villar & Lloret 2001). Although there were not many results for each density, the relative gas permeability tended to be lower for higher dry densities. The values of relative gas permeability thus obtained during FEBEX have been plotted along with the new ones in Figure 31. Since the range of dry densities tested was between 1.5 and 1.9 g/cm$^3$, there is a large dispersion of relative permeability values when they are plotted as a function of the degree of saturation. However, if they are plotted as a function of the accessible porosity, the following empirical correlation (with a $r^2$=0.83) has been found (Figure 31, right):

$k_{rg} = 2.98\ (e(1\text{-}S_r))^{2.94}$ [12]

Finally, we could simply substitute Equation 11 in Equation 10 and obtain a general law relating relative gas permeability to degree of saturation that has been included in Figure 31 (left).

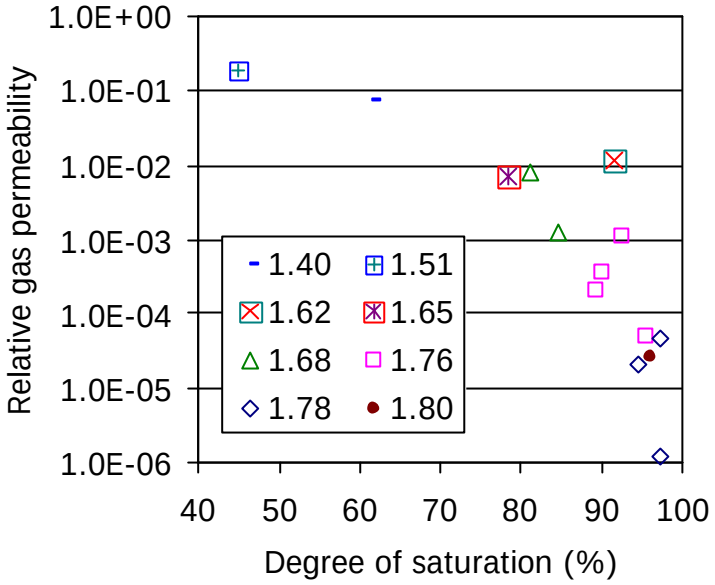


**Figure 30: Relative gas permeability deduced from the new measurements as a function of degree of saturation for different dry densities (in g/cm$^3$)**

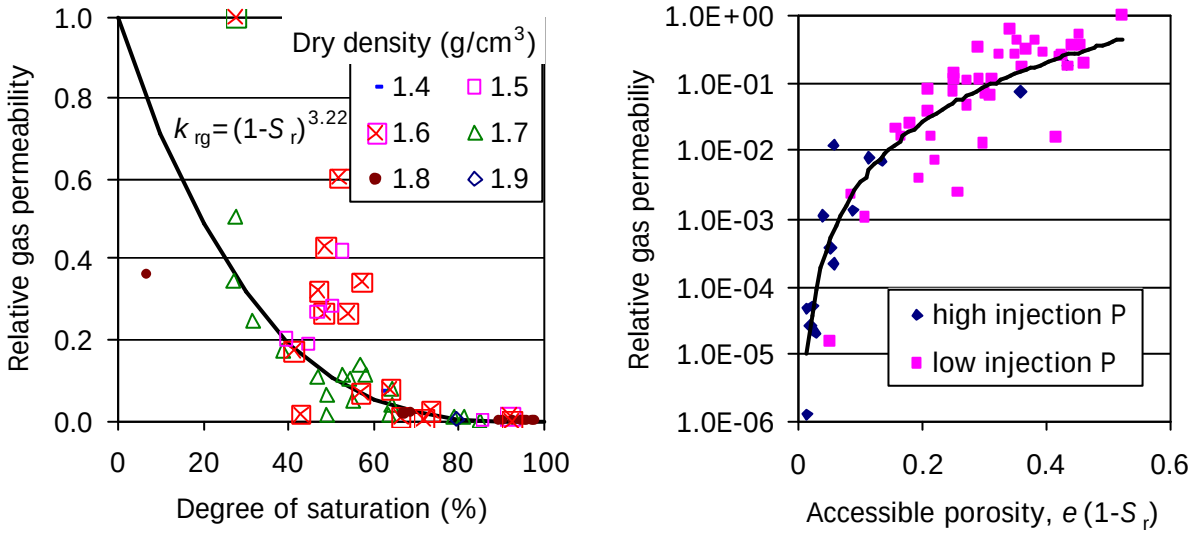


**Figure 31: Relative gas permeability computed from the tests performed with compacted FEBEX bentonite during the FEBEX and FORGE projects**

# Conclusions

The gas permeability of bentonite was greatly affected by dry density, decreasing about three orders of magnitude when it increased from 1.5 to 1.8 g/cm$^3$ for similar water content. The increase of water content caused also a decrease in gas permeability. It was found that both gas permeability and the relative gas permeability were mainly related to the accessible

porosity. These relationships could be fitted to potential expressions with exponents close to 3, as well as the relationship between intrinsic permeability and void ratio.

For gas pressures below 12 bar no effect of the injection or confining pressures on the value of permeability was detected, although when confining pressure increased from 10 to 30 bar, the permeability decreased almost two orders of magnitude. For a given confining pressure the permeability value decreased as the effective pressure increased, especially if the increase in effective pressure was due to a decrease in gas backpressure.

It was checked that the Klinkenberg effect was not significant for this material in the range of pressures applied in the tests.

Preliminary results indicated that the breakthrough pressure for the saturated bentonite with a dry density of 1.73 g/cm$^3$ was higher than 10 MPa, whereas for the saturated bentonite with a dry density slightly higher than 1.4 g/cm$^3$ was about 5 MPa. A saturated granite/bentonite interface (bentonite dry density 1.56 g/cm$^3$) allowed the passage of gas under a pressure of 0.7 MPa. After resaturation of this interface, the same breakthrough pressure was found.

# References


ENRESA, 2000. FEBEX PROJECT. Full-scale engineered barriers experiment for a deep geological repository for high level radioactive waste in crystalline host rock. Final report. *Publicación Técnica ENRESA* 1/2000, Madrid, 354 pp.

ENRESA, 2006. FEBEX Full-scale Engineered Barriers Experiment, Updated Final Report 1994-2004. *Publicación Técnica ENRESA* 05-0/2006, Madrid, 590 pp.

LLORET, A., ROMERO, E., VILLAR, M.V. 2004. FEBEX II Project Final report on thermo-hydro-mechanical laboratory tests. *Publicación Técnica ENRESA* 10/04, Madrid, 180 pp.

L'AIR LIQUIDE, 1976. *Encyclopédie des Gaz*. Amsterdam: Elsevier. 1164 pp. ISBN-10: 0444414924

LOOSVELDT, H., LAFHAJ, Z., SKOCZYLAS, F. 2002. Experimental study of gas and liquid permeability of a mortar. *Cement and Concrete Research* 32(9), 1357-1363.

SCHEIDEGGER, A.E. 1974. *The physics of flow through porous media*. 3rd ed. Toronto: University of Toronto Press, 353 pp.

VILLAR, M.V., 2002. Thermo-hydro-mechanical characterisation of a bentonite from Cabo de Gata. A study applied to the use of bentonite as sealing material in high level radioactive waste repositories. *Publicación Técnica ENRESA* 01/2002, Madrid, 258 pp.

VILLAR, M.V., LLORET, A., 2001. Variation of the intrinsic permeability of expansive clay upon saturation. 259-266 in *Clay Science for Engineering*. ADACHI, K. & FUKUE, M. (editors), Rotterdam: Balkema. ISBN 90 5809 175 9.

VILLAR, M.V., GÓMEZ-ESPINA, R., 2009. Report on thermo-hydro-mechanical laboratory tests performed by CIEMAT on FEBEX bentonite 2004-2008. *Informes Técnicos CIEMAT* 1178, Madrid, 67 pp.

VILLAR, M.V.; MARTÍN, P.L. & BARCALA, J.M. 2010. Description of experimental setups and procedures for CIEMAT gas transport tests of WP3. *Informe Técnico* CIEMAT/DMA/2G207/01/10, Madrid, 13 pp.